

Range separated hybrid density functional study of organic dye sensitizers on anatase TiO₂ nanowires

Hatice Ünal,¹ Deniz Gunceler,² Oğuz Gülseren,³ Şinasi Ellialtıoğlu,⁴ and Ersen Mete^{1,*}

¹*Department of Physics, Balıkesir University, Balıkesir 10145, Turkey*

²*Department of Physics, Cornell University, Ithaca, NY 14853, USA*

³*Department of Physics, Bilkent University, Ankara 06800, Turkey*

⁴*Basic Sciences, TED University, Ankara 06420, Turkey*

(Dated: July 8, 2014)

The adsorption of organic molecules coumarin and the donor- π -acceptor type tetrahydroquinoline (C2-1) on anatase (101) and (001) nanowires have been investigated using screened Coulomb hybrid density functional theory calculations. While coumarin forms single bond with the nanowire surface, C2-1 additionally exhibits bidentate mode giving rise to much stronger adsorption energies. Nonlinear solvation effects on the binding characteristics of the dye chromophores on the nanowire facets have also been examined. These two dye sensitizers show different electronic charge distributions for the highest occupied and the lowest unoccupied molecular states. We studied the electronic structures in terms of the positions of the band edges and adsorbate related band gap states and their effect on the absorption spectra of the dye-nanowire combined systems. These findings were interpreted and discussed from the view point of better light harvesting and charge separation as well as in relation to more efficient charge carrier injection into the semiconductor nanowire.

PACS numbers: 68.43.-h, 73.22.-f, 78.67.Uh, 88.40.jr

I. INTRODUCTION

Recently, dye sensitized solar cells (DSSC) have become an important research field in direct energy generation from sunlight. In a typical system, dye adsorbates on TiO₂ nanostructures are responsible for light harvesting with their highest occupied molecular orbitals (HOMO) residing in the band gap of the host semiconductor. The coupling of their lowest unoccupied molecular orbital (LUMO) with the conduction band (CB) of TiO₂ serves as a natural pathway for photo-generated charge injection from the dye to the CB of the substrate. The cell is then regenerated by interaction of the excited dye with a redox couple.^{1,2} The open-circuit voltage of the cell, V_{OC} , is the difference between the highest occupied level of dye-semiconductor system and redox potential of the mediator (typically iodide). For such a solar cell construction, the band positions of titania is one of the most appropriate among the other wide-bandgap semiconductors.

TiO₂, particularly the (001) surface of anatase phase, show excellent photocatalytic activity under UV irradiation.^{2,3} Sensitizer chromophores not only drive the UV-limited photoresponse of TiO₂, into the visible range but also play an important role in charge carrier dynamics. In fact, the overall cell efficiency depends on the preferable properties of dye-semiconductor composite system in relation to the factors such as the photoelectric conversion, charge carrier injection, electron-hole recombination rates and charge transport performance.

High surface-to-volume ratio of the semiconductor material is another component of the efficiency consideration. In general, TiO₂ nanoparticles provide multiple surfaces exposing large number of active sites. On the other hand, quasi-one-dimensional titania nanowires⁴ not

only accommodate even larger areas but also are superior in n-type conductivity reducing the photogenerated charge recombination rates. In the forms of nanostructures, thermodynamically the most stable phase of TiO₂ is the anatase polymorph.⁵⁻⁷ The interaction between anatase nanostructures and dye sensitizers is one of the basic issues to improve the efficiency of DSSCs.

The choice of the sensitizer dye depends not only on its durability, absorption and charge injection ability during the energy conversion cycles, but also on its production cost and easiness. Ru based photosensitizers, reaching up to 11% efficiencies (under AM 1.5 illumination), constitute an important part of the dye complexes that are used in DSSC technology.^{1,8-15} Research has been focused on finding alternatives to those well-known, metal-driven and relatively more expensive dye sensitizers.¹⁶ Several organic dye molecules have been shown to be strikingly efficient in light harvesting.¹⁷⁻²⁵ For instance, indoline derivatives showed 9.52% efficiency.²⁶ High efficiencies of the Ru complexes are attributed to their high charge injection rates into the conduction band (CB) of the TiO₂ pertaining to their metal-to-ligand charge transfer ability. Novel organic donor- π -acceptor dyes like tetrahydroquinoline based C2-1^{24,25} have been proposed to achieve intramolecular charge separation.

Improvements in the dye design crucially depend on the deep understanding of the fundamental properties of the sensitizer and its interaction with the nanostructured semiconductor. Quantitatively, novel organic dye molecules with advanced chemical and physical properties can be tailored with the aid of theoretical modeling.^{27,28} Theoretical studies have focused on the prediction of the electronic structure of the chromophores and of their interface with the TiO₂ substrates.²⁹⁻³⁹ In particular, the family of tetrahydroquinoline derived

TABLE I: Calculated adsorption energies of dye-nanowire systems (in eV)

Dye	@ (001)				@ (101)			
	PBE	HSE	PBE+PCM ^a	PBE+PCM ^b	PBE	HSE	PBE+PCM ^a	PBE+PCM ^b
Coumarin	-0.46	-0.63	-0.24	-0.05	-0.63	-0.70	-0.48	-0.23
C2-1(monodentate)	-0.72	-0.73	-0.71	-0.22	-0.57	-0.62	-0.44	-0.10
C2-1(bidentate)	-1.36	-1.25	-1.22	-0.71	-0.94	-0.83	-0.74	-0.37

^aNonlinear PCM included for CHCl₃^bNonlinear PCM included for H₂O

dyes have been studied with *ab initio* calculations.⁴⁰ O'Rourke *et al* have also considered these dyes on TiO₂(101) surface to predict their electronic structures.⁴¹

In this study, we aimed to understand the binding modes, electronic structures and optical spectra of dye sensitizers on anatase TiO₂ nanowires having (101) and (001) facets by standard as well as hybrid density functional theory (DFT) calculations. Tetrahydroquinoline based C2-1 (C₂₁H₂₀N₂SO₂) organic dyes achieving di-

rectional charge distribution upon photo-excitation have been considered as the light harvesting molecules adsorbed on the nanowires. In order to make comparisons with a simple dye molecule, we also included coumarin (C₉H₆O₂) which is extensively studied in the literature.^{26,36,42-58} Because DSSC operates in solution, the solvation effects become important. Therefore, we addressed this by using a new polarizable continuum model (PCM) for solvents with different ionicities. After briefly describing the computational methods we will discuss the results in detail.

II. COMPUTATIONAL DETAILS

In order to investigate the geometric and electronic properties of the dye and nanowire composite systems, we performed pseudo potential plane wave calculations based on standard and hybrid DFT using both Perdew-Burke-Ernzerhof (PBE)⁵⁹ and Heyd-Scuseria-Ernzerhof (HSE)⁶⁰⁻⁶² exchange-correlation (XC) functionals as implemented in the Vienna ab-initio simulation package (VASP).⁶³ The ionic cores and valence electrons with an energy cutoff value of 400 eV for the plane wave expansion were treated by projector-augmented waves (PAW) method.^{64,65} The convergence of our calculated values have been carefully tested with respect to *k*-point sampling.

In addition to the standard DFT, we used the range separated hybrid density functional approach that partially admixes exact Fock exchange and PBE exchange energies. These type of hybrids offer a better description of localized *d* states and improve the energy gap related features over the standard XC schemes. Range separated hybrid functionals tend to compensate the localization deficiency due to the lack of proper self-interaction cancellation between the Hartree and exchange terms of the pure DFT. Correct description of the adsorbate driven gap states around the band edges is critical for the estimation of the photovoltaic properties. In HSE functional, the exchange energy is separated into two parts as the long-range (LR) and the short-range (SR), as,

$$E_{\mathbf{x}}^{\text{HSE}} = a E_{\mathbf{x}}^{\text{HF,SR}}(\omega) + (1 - a) E_{\mathbf{x}}^{\text{PBE,SR}}(\omega) + E_{\mathbf{x}}^{\text{PBE,LR}}(\omega)$$

where *a* is the mixing coefficient⁶⁶ and ω is the range separation parameter.⁶⁰⁻⁶² In this approach, the correlation

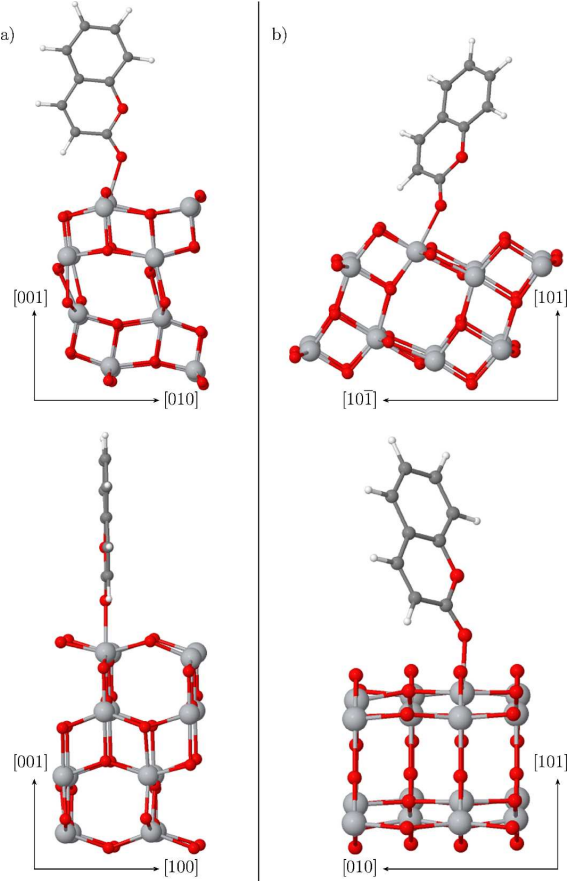


FIG. 1: Optimized adsorption geometries of coumarin on anatase (001)-nanowire (left panel) and (101)-nanowire (right panel) shown from two different viewing orientations. Here the red, light-grey, dark-grey, and white color spheres represent O, Ti, C, and H atoms, respectively.

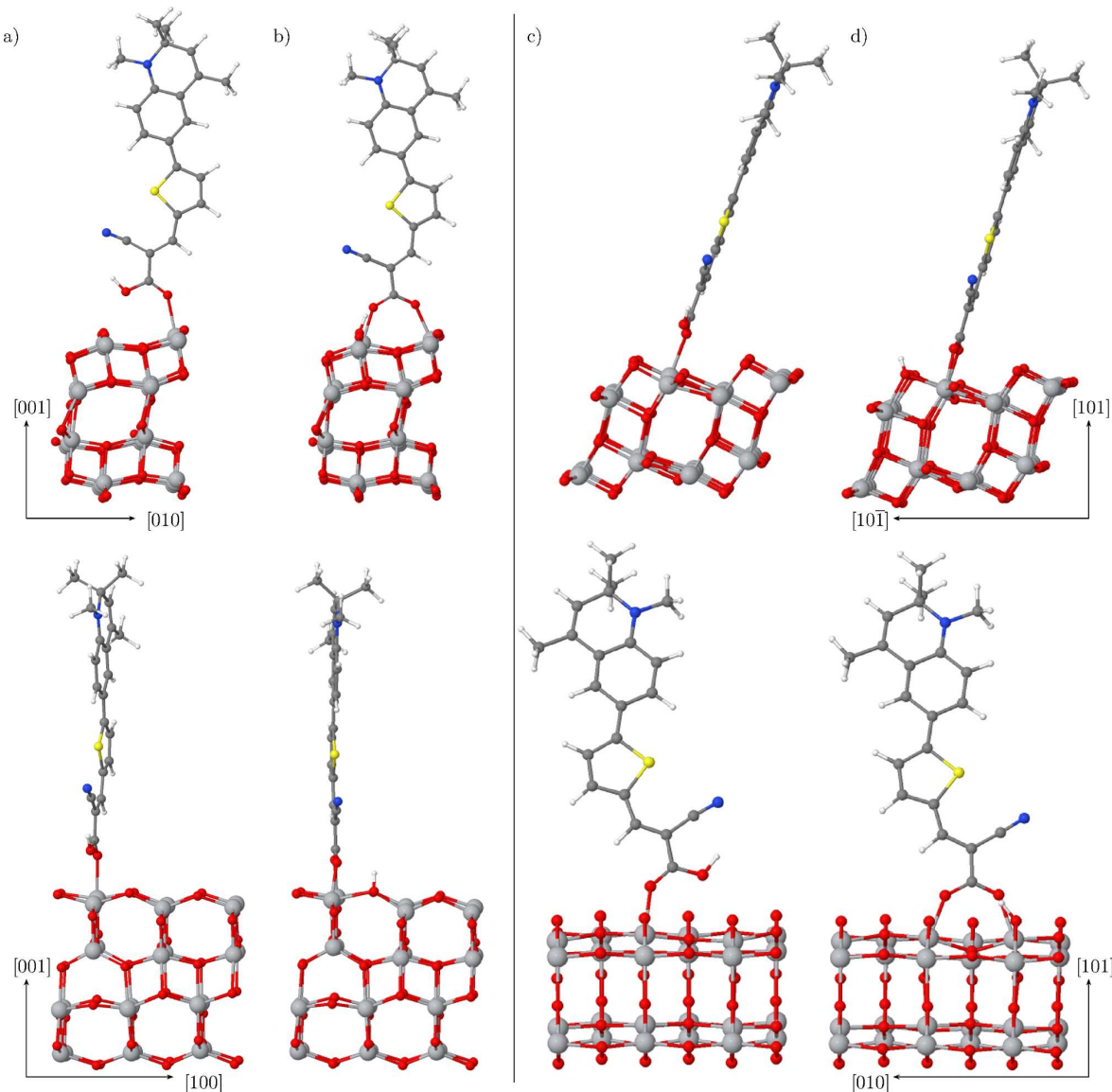


FIG. 2: Optimized adsorption geometries of C2-1 on anatase (001)-nanowire (left panel) and (101)-nanowire (right panel) with two different viewing orientations for both monodentate and bidentate bonding modes. Here the red, light-grey, dark-grey, blue, yellow and white color spheres represent O, Ti, C, N, S, and H atoms, respectively.

part of the energy is taken from standard PBE.⁵⁹

In order to study the effect of the solvent environment (chloroform and water) on the electronic structure of the dye+nw combined systems, we carried out calculations via PCM including both the new non-linear and its linear counterpart as implemented in the open-source code JDFTx.^{67–70}

In polarizable continuum models (PCM), a dielectric medium surrounding the solute molecule is generally used to reproduce the solvent environment. Therefore, free energies can be computed without the need for explicit thermodynamic sampling of the many possible different configurations of solvent molecules. The surrounding cavity of the solute is modeled by its electron density where the dielectric function of the solute turns on around a crit-

ical density value. In order to reproduce experimental solvation energies, we parametrize the critical electron density, and the effective tension in the solute-solvent interface, accordingly.^{68,69} The nonlinear⁶⁸ PCMs are advantageous over linear ones since the nonlinear models also incorporate the dielectric saturation effect. In other words, the rotational contribution to the dielectric function decreases with increasing external field. For this, we separate out the rotational contributions from electronic/vibrational contributions, and model the former as a field of interacting dipoles. For a more detailed discussion of PCMs, we refer the reader to the respective reference.⁶⁸

The stoichiometric nanowire models with (001) and (101) facets were built from the anatase form of bulk

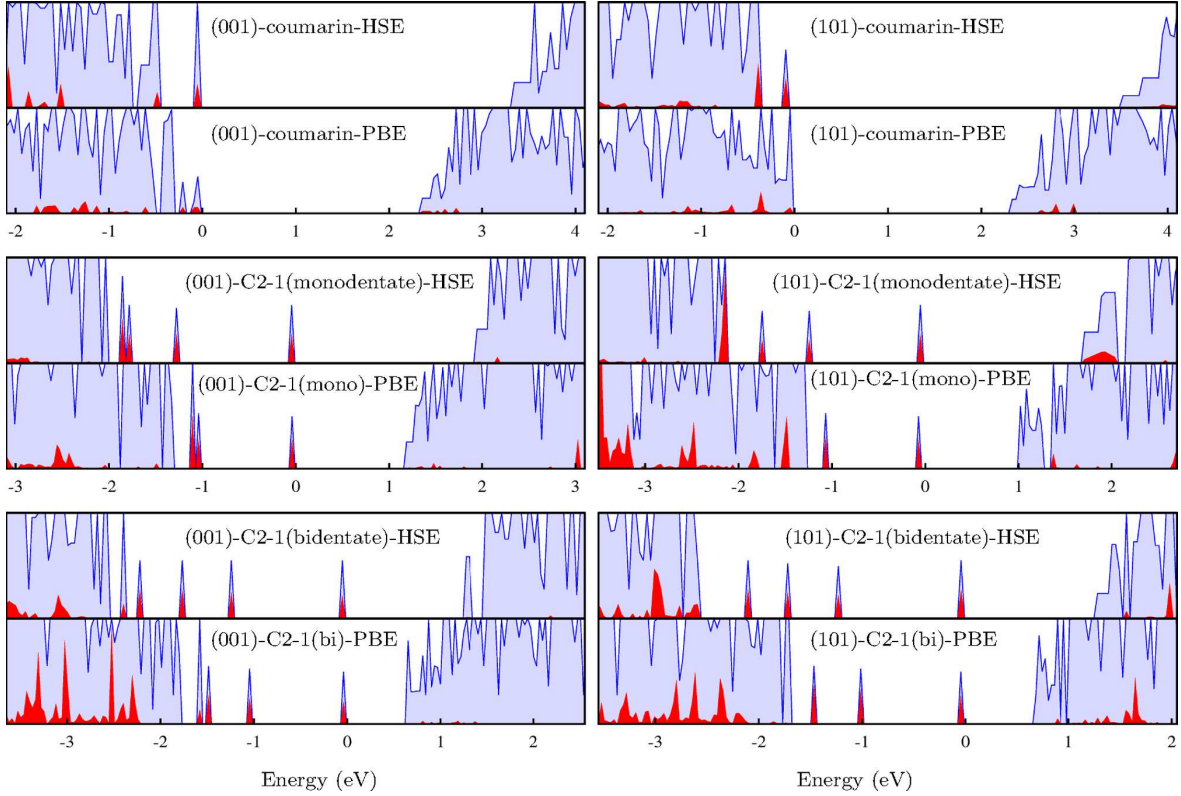


FIG. 3: Density of states (DOS) of dye-nanowire combined systems. The contribution of the dye molecules are denoted as red shades by projecting on the dye molecular orbitals. The zero of the energy is set at the highest occupied energy level.

TiO₂, referred as nw(001) and nw(101), respectively. Our tests show that the passivation of the facets are not required. Bare and dye adsorbed nanowire models are placed in periodic tetragonal super cells. In order to prevent interaction with the periodic images of the structures a sufficiently large vacuum space of at least 20 Å thick perpendicular to the nanowire axis has been inserted. Similarly, periodicity is enlarged along the nanowire axis such that the dye adsorbate can be assumed as isolated. The Hellman–Feynmann forces on each atom have been minimized (< 0.01 eV/Å) based on the conjugate-gradients algorithm to fully optimize the initial geometries. The optimized nanowire models have maintained the anatase structure as discussed in detail previously elsewhere.⁷¹

III. RESULTS & DISCUSSION

The coumarin core (C₉H₆O₂) has been focused on as a candidate sensitizer for creating highly efficient DSSCs by many experimental and theoretical works.^{26,36,42–58} First of all, the adsorption of coumarin core on the TiO₂ nanowires has been investigated as a minimal atomistic model to understand dye sensitization within the framework of total energy DFT calculations. We considered the coumarin molecule at various adsorption sites on the

(001) and (101) facets of the anatase nanowires. The energetically favorable binding modes of coumarin for both of the cases are presented in Fig. 1. Because of the tail oxygen of coumarin interacting with a five-fold coordinated surface Ti, the dye molecule aligns perpendicularly on both of the nanowire types forming a single bond (monodentate binding). Adsorption of coumarin does not cause noticeable distortion on the nanowire structure in both of the case. The length of the bond between the surface and the dye is 2.18 Å and 2.21 Å in the cases of nw(101) and nw(001), respectively.

In the case of C2-1 dyes, the tail oxygen and the OH group play an important role in the adsorption on the nanowire surfaces. The optimized geometries of different binding modes of C2-1 on TiO₂ nanowires are shown in Fig. 2. It portrays two different adsorption modes. Similar to the coumarin case, one of them is the monodentate binding in which the tail oxygen forms a single bond with the surface Ti atom giving C2-1 a perpendicular orientation with respect to the nanowire axis. In the second one, in addition to the O-Ti bond, the OH group loses the H to the nearest surface oxygen site enabling the formation of a second O-Ti bond between the dye and the nanowire. This bidentate mode is a chemical binding and so is much stronger than the monodentate case. For both of the nanowire types, the monodentate bond length is slightly larger than bidentate formation

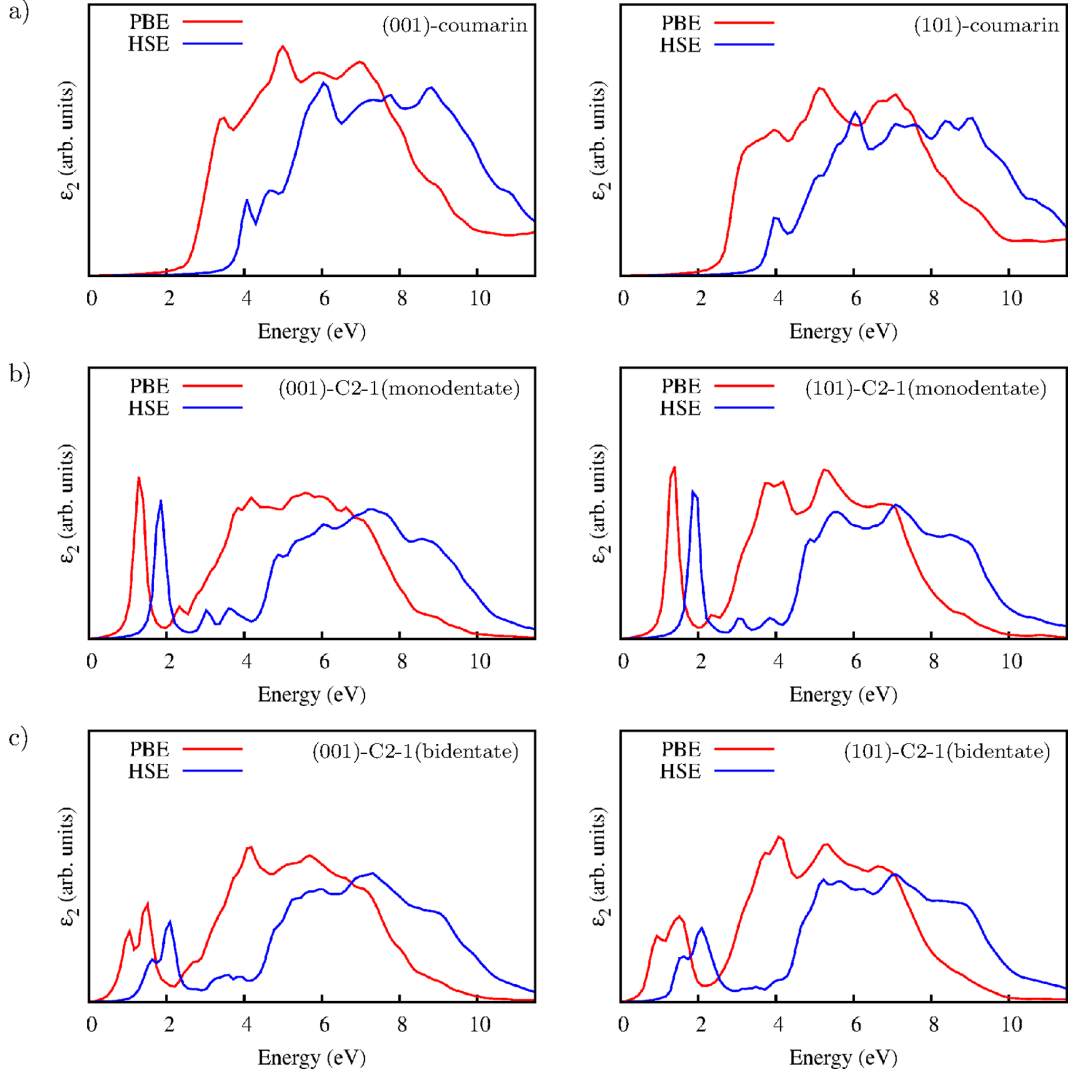


FIG. 4: Absorption Spectra for (a) Coumarin on anatase (001)-nanowire and (101) (b) C2-1 monodentate bridging on anatase (001)-nanowire and (101)-nanowire (c) C2-1 bidentate bridging on anatase (001)-nanowire and (101)-nanowire, respectively

where the bond lengths are ~ 2.0 Å which is a typical value of the bulk structures. The adsorption of C2-1 only leads to a minor change in the local environment on the nw(001). However, the surface oxygen on the nw(101) in between the two Ti atoms forming the bidentate bonds slightly buckles down as seen in Fig. 2d.

We calculated the binding energies with a standard formulation as given in previous studies.^{27,28} These values are computed using PBE and HSE schemes and are presented in Table I. The solvent effects with chloroform and water solutions have also been included on PBE results. Single bonding gives moderate and similar binding energies for both of the dyes on the two nanowire surface types. Regarding the binding energies, HSE functional yields similar values compared to the PBE ones. Strong solution effects are found to be drastically weakening the adsorption of the dye on the nanowire surface. This could indicate an expectation of low efficiencies for singly

bound molecular cases because of the reduced stability. When the binding energies of the dyes on the nanowires in Table I are considered, one can say that the dissolution of the simple coumarin dye in the electrolyte is probable in applications which causes noticeable decrease in the photovoltaic performance of DSSCs. However, the formation of the second bond as a result of the loss of the H in the OH group in the bidentate case of C2-1 dye enhances the binding appreciably. This bidentate mode of C2-1 gives the strongest binding energy among the cases considered here. Our PBE-calculated value of 0.94 eV on nw(101) is in good agreement with GGA predicted binding energy of the isolated adsorption of the molecule on (101) slab surface by O'Rourke *et al.*⁴¹ The slight buckling of the surface oxygen on nw(101) brings an energetic penalty on the binding energy of C2-1 bidentate mode which leads to a reduction of the adsorption energy compared to that of the nw(001) case. Our results suggest

that C2-1 is losing the H from its tail OH group to the nanowire surface to form a chemical bond. Therefore, it survives in a strongly ionic solution like water without dissociation.

The density of states (DOS) of the dye+nanowire combined systems have been presented in Fig. 3. Our TiO₂ nanowire models having diameters around 1 nm possess larger band gap values relative to the bulk and surface structures as a result of the quantum confinement effect.⁷¹ In general, most of the deep lying occupied molecular orbitals stay in the valence band as a resonant state. Most importantly, a number of dye-related isolated and occupied states appear above the VB edge within the band gap, depending on the nature of the binding. As a result, the Fermi energy shifts up to higher energies leading to a energy gap narrowing which is an important factor for photovoltaic properties. Moreover, the lowest lying unoccupied molecular levels of the dyes delocalizes on the Ti 3*d* states inside the conduction band (CB) of the nanowires. HSE functional corrects the band gap underestimation which is inherent in the standard PBE XC scheme. The PBE-bandgaps of bare nw(101) and nw(001) are 2.51 eV and 2.69 eV, respectively. HSE method gives an energy correction of 1.50 eV for nw(101) and 1.37 eV for the nw(001). This opening of the gap results in molecular states to fall in the energy gap, which were previously to be in resonance with the VB at the PBE level. In order to compare PBE and HSE calculated DOS structures, we aligned them with respect to their deep core energy states. For both of the nanowires, the molecular states of coumarin appear around the VB edge while one of them is isolated from the rest in the case of HSE. For C2-1 monodentate mode, PBE predicts two isolated states above the VB. Due to the gap opening by HSE functional, one more filled isolated state falls in the band gap of both of the nanowire types. On going from monodentate to bidentate bonding, there appears an additional isolated state above the VB. In the case of C2-1 bidentate mode, the positions and the number of dye related energy levels calculated with the PBE functional are in agreement with the GGA results of O'Rourke *et al.*⁴¹ The only difference comes from the alignment of TiO₂ energy bands with respect to the energy levels of the dye, which stems from our nanowire and their slab calculations. Significant band gap reduction is obtained in the case of C2-1 on both of the nanowires which is important for light harvesting.

The absorption spectra of the sensitizers, coumarin and C2-1, on nw(001) and nw(101) have been calculated at the PBE and HSE levels using the formulation as described in our previously study on the bare anatase nanowires.⁷¹ The dye related contributions in the optical spectra show similar characteristics with both PBE and HSE calculations as shown in Fig. 3. These features correspond to the first absorption peaks in each case associated with excitations from the highest occupied molecular states to the unoccupied molecular states which are coupled to the CB of the semiconductor. Sim-

ilar absorption properties are obtained in the UV region, which are mostly related with the interband transitions from the VB to the CB states. Although the main characteristics are alike, PBE-calculated spectra is significantly red shifted with respect to that of the HSE due to the local density approximation (LDA) giving rise to an inherent underestimation of the band gap of TiO₂. The coumarin core brings the lowest lying peak which extends the absorption threshold slightly into the visible region as seen in Fig. 4a for both of the nanowire types. The C2-1+nanowire combined system has more favorable optical properties than the coumarin+nanowire structures. A distinct and strong absorption peak results due to the excitation from the occupied molecular state at the Fermi energy to the frontier unoccupied molecular state which delocalizes inside the CB of the semiconductor. As being a D- π -A type dye, such an excitation achieves charge redistribution from the donor to the acceptor moiety of C2-1 dye which is important for the charge injection into the CB of TiO₂. This peak associated with the charge transfer (CT) state is identified at ~ 2 eV at the HSE level while PBE prediction falls in the near infrared (IR) part of the spectrum. In the energetically the most preferable bidentate bonding mode of C2-1 sensitizer, two absorption peaks are identified which are significantly broadened in the visible range. This is reminiscent of the chemical nature of the adsorption of C2-1 on both the (001) and the (101) surfaces of the anatase nanowire. The first absorption peak positions of C2-1 on the anatase nanowire structures calculated at the HSE level are slightly red shifted compared with respect to the experimental data^{24,25} of Chen *et al.* obtained on nanocrystalline TiO₂. Consequently, based on our hybrid DFT computations, the bidentate bonding form of C2-1 on TiO₂ survives in solution, causes a number of isolated filled molecular states to appear in the band gap, functionalizes the anatase nanowires to absorb a wide range of the visible region and achieves charge separation which is promising for both the enhancement of the charge injection efficiencies and for the reduction of the charge carrier recombination rates.

IV. CONCLUSIONS

The binding geometries, electronic structures and absorption characteristics of two organic molecules on TiO₂ nanowires with (101) and (001) facets have been investigated using screened Coulomb hybrid density functional calculations. Coumarin causes new gap states to appear at edge of the VB of the nanowires. These systems that we chose as the minimal dye+nanowire models result in a narrowing of the electronic band gap of TiO₂. Strong bidentate binding of tetrahydroquinoline C2-1 dye brings a number of isolated and occupied gap states that both result in a significant narrowing of the band gap and cause a broader absorption structure functionalizing the semiconductor nanowires in whole visible

region. Nonlinear solvent effects suggest that the dissolution of coumarin and monodentate binding of C2-1 from the nanowires is probable in an actual electrolyte. Bidentate adsorption of donor- π -acceptor type C2-1 molecules can achieve directional charge transfer excitation to increase charge injection probabilities, allow absorption in the full range of visible spectrum to achieve enhanced light harvesting, and exhibit strong binding to reduce degradation of possible device operation.

Acknowledgments

This work is supported by TÜBİTAK, The Scientific and Technological Research Council of Turkey (Grant #110T394). Computational resources were provided by ULAKBİM, Turkish Academic Network & Information Center.

-
- * Electronic address: emete@balikesir.edu.tr; Corresponding author
- ¹ B. O'Regan and M. Grätzel, *Nature* **353**, 737 (1991).
 - ² A. Fujishima and K. Honda, *Nature (London)* **238**, 37 (1972).
 - ³ A. Fujishima, X. T. Zhang, and D. A. Tryk, *Surf. Sci. Rep.* **63**, 515 (2008).
 - ⁴ D. Çakır and O. Gülseren, *Phys. Rev. B* **80**, 125424 (2009).
 - ⁵ P. K. Naicker, P. T. Cummings, H. Zhang and J. F. Banfield, *J. Phys. Chem. B* **109**, 15243-15249 (2005).
 - ⁶ A. Iacomino, G. Cantele, F. Trani, and D. Ninno, *J. Phys. Chem. C* **114**, 12389-12400 (2010).
 - ⁷ V. C. Fuertes, C. F. A. Negre, M. B. Oviedo, F. P. Bonafé, F. Y. Oliva, and C. G. Sánchez, *J. Phys. Condens. Matter* **25**, 115304 (2013).
 - ⁸ M. K. Nazeeruddin, A. Kay, I. Rodicio, R. Humphry-Baker, E. Müller, P. Liska, N. Vlachopoulos, and M. Grätzel, *J. Am. Chem. Soc.* **115**, 6382 (1993).
 - ⁹ Y. Tachibana, J. E. Moser, M. Grtzel, D. R. Klug, and J. R. Durrant, *J. Phys. Chem.* **100**, 20056-20062 (1996).
 - ¹⁰ D. W. Thompson, J. F. Wishart, B. S. Brunshwig, and N. Sutin, *J. Phys. Chem. A* **105**, 8117 (2001).
 - ¹¹ S. Nakade, W. Kubo, Y. Saito, T. Kamzaki, T. Kitamura, Y. Wada, and S. J. Yanagida, *J. Phys. Chem. B* **107**, 14244 (2003).
 - ¹² P. Wang, S. M. Zakeeruddin, J. E. Moser, M. K. Nazeeruddin, T. Sekiguchi, and M. Grätzel, *Nat. Mater.* **2**, 402 (2003).
 - ¹³ G. Benkö, J. Kallioinen, P. Myllyperki, F. Trif, J. E. I. Korppi-Tommola, A. P. Yartsev, and V. Sundstrm, *J. Phys. Chem. B* **108**, 2862-2867 (2004).
 - ¹⁴ P. Wang, C. Klein, R. Humphry-Baker, S. Zakeeruddin, and M. Grätzel, *Appl. Phys. Lett.* **86**, 123508 (2005).
 - ¹⁵ M. K. Nazeeruddin, F. De Angelis, S. Fantacci, A. Selloni, G. Viscardi, P. Liska, S. Ito, B. Takeru, and M. Grätzel, *J. Am. Chem. Soc.* **127**, 16835 (2005).
 - ¹⁶ A. Mishra, M. K. R. Fischer, and P. Bäuerle, *Angew. Chem. Int. Ed.* **48** 2474-2499 (2009).
 - ¹⁷ A. C. Khazraji, S. Hotchandani, S. Das, and P. V. Kamat, *J. Phys. Chem. B* , **103**, 4693 (1999).
 - ¹⁸ K. Sayama, K. Hara, N. Mori, M. Satsuki, S. Suga, S. Tsukagoshi, Y. Abe, H. Sugihara, and H. Arakawa, *Chem. Commun.* 1173 (2000).
 - ¹⁹ K. Hara, Z. Wang, T. Sato, A. Furube, R. Katoh, H. Sugihara, Y. Dan-oh, C. Kasada, A. Shinpo, and S. Suga, *J. Phys. Chem. B* **109**, 15476 (2005).
 - ²⁰ Z. Wang, Y. Cui, Y. Dan-oh, C. Kasada, A. Shinpo, and K. Hara, *J. Phys. Chem. C* **112**, 17011 (2008).
 - ²¹ H. Qin, S. Wenger, M. Xu, F. Gao, X. Jing, P. Wang, S. M. Zakeeruddin, and M. Grätzel, *J. Am. Chem. Soc.* **130**, 9202 (2008).
 - ²² N. Koumura, Z. Wang, S. Mori, M. Miyashita, E. Suzuki, and K. Hara, *J. Am. Chem. Soc.* **128**, 14256 (2006); correction: **130**, 4202 (2008).
 - ²³ X. Jiang, T. Marinado, E. Gabrielsson, D. P. Hagberg, L. Sun, and A. Hagfeldt, *J. Phys. Chem. C* **114**, 2799 (2010).
 - ²⁴ R. Chen, X. Yang, H. Tian, X. Wang, A. Hagfeldt, and L. Sun, *Chem. Mater.* **19** 4007-4015 (2007).
 - ²⁵ R. Chen, X. Yang, H. Tian, and L. Sun, *J. Photochem. Photobiol. A: Chemistry* **189** 295-300 (2007).
 - ²⁶ S. Ito, H. Miura, S. Uchida, M. Takata, K. Sumioka, P. Liska, P. Comte, P. Pëchy, and M. Grätzel, *Chem. Comm.* 5194 (2008).
 - ²⁷ D. Çakır, O. Gülseren, E. Mete, and Ş. Ellialtıoğlu, *Phys. Rev. B* **80**, 035431 (2009).
 - ²⁸ D. Çakır, O. Gülseren, E. Mete, and Ş. Ellialtıoğlu, *J. Phys. Chem. C* **115**, 9220-9226 (2011).
 - ²⁹ C. Daul, E. J. Baerends, and P. Vernooijs, *Inorg. Chem.* **33**, 3538-3543 (1994).
 - ³⁰ G. Brocks and A. Tol, *J. Phys. Chem.* **100**, 1838-1846 (1996).
 - ³¹ K. Naito, M. Sakurai, and S. Egusa, *J. Phys. Chem. A* **101**, 2350-2357 (1997).
 - ³² S. I. Gorelsky and A. B. P. Lever, *J. Organomet. Chem.* **635**, 187-196 (2001).
 - ³³ W. Stier and O. V. Prezhdo, *J. Phys. Chem. B* **106**, 8047-8054 (2002).
 - ³⁴ P. Acebal, S. Blaya, and L. Carretero, *Chem. Phys. Lett.* **374**, 206-214 (2003).
 - ³⁵ W. F. Pasveer, P. A. Bobbert, M. A. J. Michels, B. M. W. Langeveld-Voss, H. F. M. Schoo, and J. J. A. M. Bastiaansen, *Chem. Phys. Lett.* **381**, 392-396 (2003).
 - ³⁶ K. Hara, T. Sato, R. Katoh, A. Furube, Y. Ohga, A. Shinpo, S. Suga, K. Sayama, H. Sugihara, and H. Arakawa, *J. Phys. Chem. B* **107**, 597-606 (2003).
 - ³⁷ J. Banuelos Prieto, F. Lopez Arbeloa, V. Martinez Martinez, and I. Lopez Arbeloa, *Chem. Phys.* **296**, 13-22 (2004).
 - ³⁸ L. Campbell and S. Mukamel, *J. Chem. Phys.* **121**, 12323 (2004).
 - ³⁹ P. Persson, M. J. Lundqvist, R. Ernstorfer, W. A. Goddard III, and F. Willig, *J. Chem. Theory Comput.* **2**, 441-451 (2006).
 - ⁴⁰ C.-R. Zhang, L. Liu , J.-W. Zhe, N.-Z. Jin, Y. Ma, L.-H. Yuan, M.-L. Zhang, Y.-Z. Wu, Z.-J. Liu, and H.-S. Chen, *Int. J. Mol. Sci.* **14** 5461-5481 (2013).
 - ⁴¹ C. O'Rourke and D. R. Bowler *J. Phys. Chem. C* **114**, 20240-20248 (2010).

- ⁴² Z.-S. Wang, F.-Y. Li, C.-H. Huang, L. Wang, M. Wei, L.-P. Jin, and N.-Q. Li, *J. Phys. Chem. B* **104**, 9676 (2000).
- ⁴³ A. Ehret, L. Stuhl, and M. T. Spitler, *J. Phys. Chem. B* **105**, 9960 (2001).
- ⁴⁴ Z.-S. Wang, F.-Y. Li, and C.-H. Huang, *J. Phys. Chem. B* **105**, 9210 (2001).
- ⁴⁵ P. Wang, S. M. Zakeeruddin, R. Humphry-Baker, J. E. Moser, and M. Grätzel, *Adv. Mater.* **15**, 2101 (2003).
- ⁴⁶ P. Wang, S. M. Zakeeruddin, P. Comte, R. Charvet, R. Humphry-Baker, and M. Grätzel, *J. Phys. Chem. B* **107**, 14336 (2003).
- ⁴⁷ T. Horiuchi, H. Miura, K. Sumioka, and S. Uchida, *J. Am. Chem. Soc.* **126**, 12218 (2004).
- ⁴⁸ T. Kitamura, M. Ikeda, K. Shigaki, T. Inoue, N. A. Anderson, X. Ai, T. Lian, and S. Yangagida, *Chem. Mater.* **16**, 1806 (2004).
- ⁴⁹ Z.-S. Wang, K. Sayama, and H. Sugihara, *J. Phys. Chem. B* **109**, 22449 (2005).
- ⁵⁰ D. P. Hagberg, T. Edvinsson, T. Marinado, G. Boschloo, A. Hagfeldt, and L. Sun, *Chem. Commun.* 2245 (2006).
- ⁵¹ S.-L. Li, K.-J. Jiang, K.-F. Shao, and L.-M. Yang, *Chem. Commun.* 2792 (2006).
- ⁵² Y. Chiba, A. Islam, Y. Watanabe, R. Komiya, N. Koide, and L. Han, *Jpn. J. Appl. Phys.* **45**, L638 (2006).
- ⁵³ Z.-S. Wang, Y. Cui, K. Hara, Y. Dan-oh, C. Kasada, and A. Shinpo, *Adv. Mater.* **19**, 1138-1141 (2007).
- ⁵⁴ Y. Kurashige, T. Nakajima, S. Kurashige, and K. Hirao, *J. Phys. Chem. A* **111**, 5544-5548 (2007).
- ⁵⁵ J. Preat, P. -F. Loos, X. Assfeld, D. Jacquemin, and E. A. Perpète, *J. Mol. Struct. Theochem.* **808**, 85-91 (2007).
- ⁵⁶ X. Zhang, J. -J. Zhang, and Y. -Y. Xia, *J. Photochem. Photobiol. A Chem.* **194**, 167-172 (2008).
- ⁵⁷ R. Sanchez-de-Armas, M. A. San Miguel, J. Oviedo, and J. F. Sanz, *Phys. Chem. Chem. Phys.* **14**, 225-233 (2012).
- ⁵⁸ C. I. Oprea, P. Panait, F. Cimpoesu, M. Ferbinteanu, and M. A. Girtu, *Materials* **6**, 2372-2392 (2013).
- ⁵⁹ J. P. Perdew, K. Burke, and M. Ernzerhof, *Phys. Rev. Lett.* **77**, 3865 (1996).
- ⁶⁰ J. Heyd, G. E. Scuseria, and M. Ernzerhof, *J. Chem. Phys.* **118**, 8207 (2003).
- ⁶¹ J. Heyd, G. E. Scuseria, and M. Ernzerhof, *J. Chem. Phys.* **124**, 219906 (2006).
- ⁶² J. Paier, M. Marsman, K. Hummer, G. Kress, I. C. Gerber, and J. G. Angyan, *J. Chem. Phys.* **125**, 249901 (2006).
- ⁶³ G. Kresse and J. Hafner, *Phys. Rev. B*, **47**, 558 (1993).
- ⁶⁴ P. E. Blöchl, *Phys. Rev. B* **50**, 17953 (1994).
- ⁶⁵ G. Kresse and J. Joubert, *Phys. Rev. B* **59**, 1758 (1999).
- ⁶⁶ J. P. Perdew, M. Ernzerhof, and K. Burke, *J. Chem. Phys.* **105**, 9982 (1996).
- ⁶⁷ K. Letchworth-Weaver and T. A. Arias, *Phys. Rev. B.*, **86**, 075140 (2012).
- ⁶⁸ D. Gunceler, K. Letchworth-Weaver, R. Sundararaman, K.A. Schwarz and T.A. Arias, *Modelling Simul. Mater. Sci. Eng.* **21** 074005 (2013).
- ⁶⁹ D. Gunceler, and T. A. Arias. preprint available at arXiv:1403.6465
- ⁷⁰ R. Sundararaman, D. Gunceler, K. Letchworth-Weaver, and T. A. Arias. *JDFTx*. <http://jdf.tx.sourceforge.net>, (2012).
- ⁷¹ H. Ünal, O. Gülseren, Ş. Ellialtıoğlu, and E. Mete, *Phys. Rev. B* **89**, 205127 (2014).